Calculation of the flow around hydrofoils at moderate Reynolds numbers

Rui Miguel Alves Lopes
rui.a.lopes@tecnico.ulisboa.pt

Instituto Superior Técnico, Lisboa, Portugal

December 2015

Abstract

The effect of laminar to turbulent flow transition region, which can be responsible for important features at low Reynolds numbers flows, is not captured by common turbulence models, and thus ignored in most numerical calculations. Recently a new transition model presenting promising results has been proposed - the $\gamma - Re_\theta$ model. This model is easily implemented in modern codes which resort to non-structured grids, unlike the alternatives used until now. The goal of this paper is to study the behaviour of this model, assessing its numerical robustness and comparing the obtained solution with experimental results and a baseline solution that uses the already extensively validated $k - \omega$ SST turbulence model. As a preliminary calculation, the flow over a zero pressure gradient flat plate was analysed, to study the effect of the inlet turbulent quantities. On a second stage the flow over three different airfoils was simulated, in order to evaluate the improvement of the results obtained due to the additional model. The results obtained show that the new model is capable of capturing laminar separation bubbles and natural transition, improving the modelling accuracy in most cases. However, its numerical behaviour presents poor characteristics due to higher difficulties with iterative convergence and higher influence of the discretization error. The model also suffers from a high sensitivity to the turbulence inlet conditions, aggravated by the overestimated decay of the turbulence model variables.

Keywords: Transition, Reynolds Equations, Airfoils, Computational Fluid Dynamics, Turbulence Models

1. Introduction

In the recent years, there has been an increasing focus on numerical simulations: these consist in the discretization of the governing equations using one of several approaches [1] such as finite differences, finite volume and finite elements, giving rise to the field of Computational Fluid Dynamics (CFD).

CFD presents itself as an attractive option due to the wealth of data that can be obtained. Additionally, the constant growth in processing and memory capabilities makes it an engineering tool, as increasingly accurate and detailed solutions are calculated.

Due to its physics, the turbulent regime has been one of the greatest challenges for CFD. Nevertheless, good results are obtained nowadays for the turbulent flow region due to the wealth of existing turbulence models, which have been extensively validated, covering a wide range of applications.

As such, the next step is to accurately model the transition region from laminar to turbulent flow, as it can be responsible for important features of the flow. The currently used turbulence models such as $k - \omega$ and $k - \epsilon$ models fail to model transition accurately.

Transition is relevant for the flow characteristics in low Reynolds number applications. Although large transport aircraft usually deal with high Reynolds numbers, over 10^7, unmanned aerial vehicles (UAVs) and micro air vehicles (MAVs) operate in the low Reynolds number range: 10^5 to 10^6 [2]. These UAVs can be used for a variety of purposes, such as aircraft tracking, weather monitoring and ocean surveillance [3, 4]. The development of wind energy systems is another growing area where low Reynolds number phenomena is relevant, due to the increasing attention and investment in this particular renewable energy source, which requires efficient solutions: the airfoil section is critical for the determination of the loads that the structure is subjected to.

There are methods to achieve good accuracy regarding transition for simple flows, such as DNS approaches. Another alternative for 2-D geometries is the e^n method [5, 6] used in the X-FOIL code of Drela and Giles [7]. However, these options are limited in their usefulness: the use of DNS calculations is still very resource demanding and the remaining methods are not easily introduced in modern CFD codes.

Recently, in 2006, a new transition model was published: the $\gamma - Re_\theta$ model proposed by Langtry et al. [8]. This model seems to provide a good basis to incorporate the transition region in RANS simulations, compatible with modern CFD characteristics: applicable to unstructured grids and parallel computation due to its local formulation.

The goal of this article is to study the influence of transition modelling on the flow over three different airfoils, by performing a verification and validation exercise, using the

flow solver ReFRESCO [9] along with the $\gamma - Re_\theta$ model. The results regarding drag and lift coefficients, as well as pressure distributions are then compared to available experimental data, as part of the validation stage. For each airfoil, two sets of calculations will be done: one using only the $k-\omega$ Shear Stress Transport (SST) turbulence model and another using the previously mentioned γ - Re_θ transition model, which is coupled with the SST model. The two cases shall be compared, in order to understand the changes in the solution, provided by the transition model, and the potential improvement in accuracy regarding the lift and drag coefficients.

The following describes the structure of this paper: section 2 discusses briefly the mathematical models behind the RANS approach, mentioning a brief overview of some transition models. Section 3 is dedicated to all the numerical aspects concerning the airfoil calculations. Finally, the results obtained for each of the airfoils studied are presented and discussed in section 4. The conclusions drawn from this work are presented in section 5, as well as considerations and suggestions for future studies on the subject.

2. Background

Many different options exist for the simulation of fully turbulent flows. Depending on the application, some models perform better than others due to the calibration of the constants but, overall, it is possible to obtain good results if choosing the appropriate model. However, the development of turbulence models has focused only on the fully turbulent flow region, thus the transition phenomena is not correctly modelled, and whenever its influence is important - for example on low Reynolds numbers applications - turbulence models fail to capture its effect. Unlike turbulence there still is not a wide range of models which produce adequate results for various applications.

The difficulty in modelling transition arises from its non-linearity, wide range of scales at play, and the fact that it can occur through different mechanisms, depending on the application. Natural transition occurs when the freestream turbulence level is low (<1%) and Tollmien-Schlichting waves grow and become unstable, originating turbulent spots which further erupt into a fully turbulent regime [10]. When the freestream turbulence level is high (>1%), typical of turbomachinery flows, the first stages of natural transition are bypassed, and turbulent spots are produced due to freestream disturbances [11] - bypass transition. Separation induced transition [12] occurs when an adverse pressure gradient causes a laminar boundary layer to separate. In the separated shear layer it is possible for transition to develop and the flow becomes turbulent, occasionally reattaching to the wall, due to the increased mixing capability of the flow, forming a laminar separation bubble.

Nevertheless, there are several options in order to model this phenomena [13]. The first approach is based on stability theory, in which the continuity and momentum equations are linearized and a form is assumed for a single disturbance. This is the basis for the much used e^n method [5, 6], used in the popular X-FOIL code [7]. Despite providing good results, this method is only applicable to simple geometries, and cannot be easily implemented in modern CFD codes due to the non-local operations involved.

DNS and LES (Large Eddy Simulation) [14] are also valid alternatives which produce good results and a large wealth of information, excessive for engineering purposes. However, considering the required computational means, they are excluded from practical applications.

Another possible alternative are low Reynolds number turbulence models [15]. However the results exhibited are strongly dependent on the calibration of the models, namely for the viscous sub-layer [16], and the physics of the phenomenon are not correctly captured.

One common approach to model transition is to make use of empirical correlations along with a transport equation for the intermittency [17]. However, they suffer from the drawback that the correlations used invoke non-local quantities such as the momentum thickness Reynolds number.

Recently, in 2006, a new alternative has been proposed by Langtry et al. [8], based on the intermittency model which avoids the usage of non-local quantities - the $\gamma - Re_\theta$ model. Two additional transport equations are used: one for intermittency and another for the transition onset Reynolds number and it is coupled with the $k-\omega$ SST turbulence model. When it was first proposed, the model lacked two main correlations which were deemed proprietary. Finally, in 2009 the full model was released to the scientific community [18]. Some efforts concerning the validation of the model and comparison of the results with well established methods such as the e^n method have already been published [19]. This is the model used in this work, chosen due to the easy implementation on modern CFD codes as well as the results presented so far. This model is also part of a new concept of transition modelling based on empirical correlations - Local Correlation-Based Transition Modelling (LCTM). This designation will be used throughout this paper to refer to the $\gamma - Re_\theta$ model.

3. Implementation

All calculations were performed with the ReFRESCO flow solver. ReFRESCO is a viscous-flow CFD code that solves multiphase (unsteady) incompressible flows using the Reynolds-Averaged Navier-Stokes equations, complemented with turbulence models, cavitation models and volume-fraction transport equations for different phases. The equations are discretized using a finite-volume approach with cell-centered collocated variables, in strong-conservation form, and a pressure-correction equation based on the SIMPLE algorithm is used to ensure mass conservation. Time integration is performed implicitly with first or second-order backward schemes. At each implicit time step, the non-linear system for velocity and pressure is linearised with Picard's method and either a segregated or coupled approach is used. A segregated ap-

proach is always adopted for the solution of all other transport equations. The implementation is face-based, which permits grids with elements consisting of an arbitrary number of faces (hexahedrals, tetrahedrals, prisms, pyramids, etc.) and if needed h-refinement (hanging nodes). State-of-the-art CFD features such as moving, sliding and deforming grids, as well as automatic grid refinement are also available. The code is parallelised using MPI and sub-domain decomposition, and runs on Linux workstations and HPC clusters. ReFRESCO is currently being developed and verified at MARIN (in the Netherlands), in collaboration with IST (in Portugal), and other universities [9].

The quality of the grid used in a calculation has a significant impact on the quality of the solution obtained after the calculation is performed. For this thesis, an existing grid generator [20] was used, resulting in structured, multi-block grids with 5 blocks: The first block is a C-shaped block around the airfoil. The second and third blocks are the top and bottom parts of the domain. The fourth block is the area upstream of the airfoil, while the last block is the area downstream of the airfoil, which captures the wake.

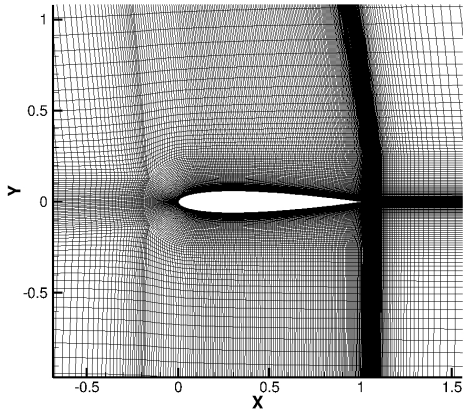

Figure 1: Coarsest grid for the NACA 0012 airfoil at $\alpha = 0$

- The inlet was located 12 chords away from the leading edge of the airfoil, where the velocity vector and turbulence quantities were given by a Dirichlet boundary condition.
- The top and bottom boundaries were located each 12 chords away from the airfoil, with a slip boundary condition.
- The outlet was located 24 chords downstream of the leading edge of the airfoil. An outflow boundary condition was imposed: derivatives with respect to x set to 0.
- The surface of the airfoil is treated as a solid wall: impermeability and no-slip conditions are used.

All calculations were performed on a set of five geometrically similar grids with different refinement levels, in which the refinement ratio was doubled between the coarsest and finest grid. They are identified by the number of points along the surface of the airfoil: the coarsest grid has 301 points, while the finest has 601 grid points. All grids obeyed the condition $y^+ < 1$, as recommended by Langtry [21] for the use of the transition model. Figure 1 (b) shows an example of one of the grids used. Performing the calculations on all 5 grids will allow for an estimation of the discretization error. The procedure is based on Richardson extrapolation, which assumes that the discretization is the only source of uncertainty. To fulfil that assumption, round-off and iterative errors should be minimized accordingly. In the present work, calculations were performed in double precision, which makes the round-off error negligible. To reduce the iterative error, the calculations ran until the maximum L_∞ residual norm for all equations was below 10^{-6} when using only the turbulence model. When the transition model was used, this was changed to 10^{-5}. To obtain an estimate for the discretization error ϵ_ϕ, it is assumed to be of the following form:

$$\epsilon_\phi = \delta_{RE} = \phi_i - \phi_o = \alpha h_i^p \tag{1}$$

Here p is the observed order of convergence, ϕ_i is the value of the variable ϕ on grid i, α is a constant and h_i is the typical cell spacing of grid i. At least three different grids are required to estimate ϵ_ϕ. However, to avoid the influence of numerical noise on the solution, more than three grids can be used. When this happens, the error estimation is performed in the least-squares sense.

The final objective is to estimate the uncertainty of a given quantity, U_ϕ, the interval which contains the exact solution with 95 % coverage,

$$\phi_i - U_\phi \leq \phi_{exact} \leq \phi_i + U_\phi \tag{2}$$

The estimation of the uncertainty is done considering the least-squares adjustment, and is complemented by a safety factor based on the reliability of the adjustment. The complete procedure is described in [22].

Turbulent decay has a significant influence over the behaviour of the turbulent quantities, which translates in a large impact when using the $\gamma - Re_\theta$ model. One option to deal with this issue [23], is to deactivate the destruction terms in the turbulence model equations, preventing the decay in the regions where the x coordinate is lower than a certain value, x_{inlet}. This approach suffers from the drawback that it may not be practical for complex geometries, and leads to one more variable that must be decided upon. Nevertheless, this was the used approach, leading to a much higher sensitivity to the inlet eddy viscosity. This method is further referred to as frozen decay.

3.1. NACA 0012

For the NACA 0012 calculations the Reynolds number was 2.88×10^6. The turbulence intensity was set to 1% for all cases. Three different combinations for the viscosity ratio

and x_{inlet} were tested. These conditions are expressed in Table 1.

Case	$\frac{\mu_t}{\mu}$	x_{inlet}
A	1.65	-0.04
B	1.65	-1
C	0.5	-0.04

Table 1: Turbulent conditions tested for the NACA 0012 airfoil

The value for the viscosity ratio for the A case was selected to match the available experimental data for the drag coefficient for the zero lift angle. Only the LCTM calculations were performed with frozen decay. The Reynolds number and selected angles of attack were chosen based on available experimental data for the pressure coefficient distributions, as well as lift and drag coefficients. [24, 25].

3.2. NACA 66-018

The Reynolds number for this airfoil was 3×10^6. Only one set of turbulent conditions was considered, which corresponds to case A of the NACA 0012 conditions: turbulence intensity set to 1%, $\frac{\mu_t}{\mu} = 1.65$ and $x_{inlet} = -0.04$. Both the LCTM and SST calculations had frozen decay. For the SST case, not much difference in the results is to be expected, but it helped the iterative convergence. As before, the angles of attack chosen were based on experimental data against which the results could be compared [26].

3.3. Eppler 387

Two different Reynolds numbers were used for the Eppler 387 airfoil: 1×10^5 and 3×10^5. Free decay occurred for both the SST and LCTM cases, and the inlet turbulent conditions were the same for either Reynolds number: turbulence intensity set to 1%, $\frac{\mu_t}{\mu} = 0.003$. The decay was not frozen for this case since the Eppler 387 forms a laminar separation bubble for the mentioned Reynolds numbers and separation-induced transition takes place. Conditions for both cases were based on wind-tunnel data [27–31].

4. Results

This sections presents the most significant results obtained for the three airfoils. The detailed results can be found on [32].

4.1. NACA 0012

Figure 2 shows the pressure coefficient distribution for all cases tested for $\alpha = 0°$. The only significant difference is a slight local increase in pressure in the region where transition occurs for each case. All conditions show good agreement with the experimental points.

The skin friction distribution for $\alpha = 0°$ is shown in Figure 3, illustrating the differences in the location of the transition point for the four solutions.

Figures 4 and 5 show the numerical and experimental locations of transition for both the upper and lower surfaces.

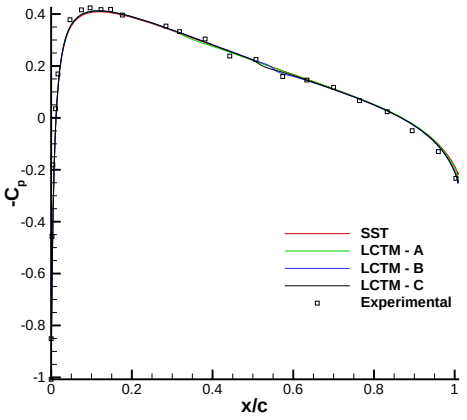

Figure 2: Pressure coefficient for the NACA 0012 airfoil, $\alpha = 0°$.

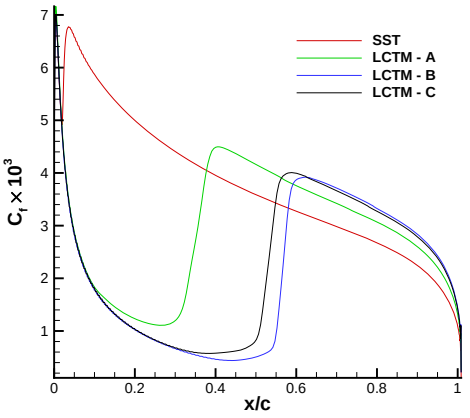

Figure 3: Skin friction for the NACA 0012 airfoil, $\alpha = 0°$.

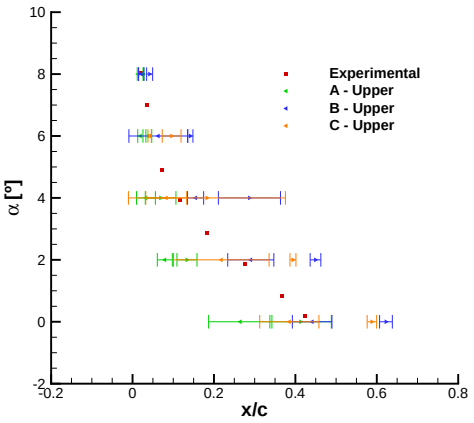

Figure 4: Transition location for the NACA 0012 airfoil, upper surface.

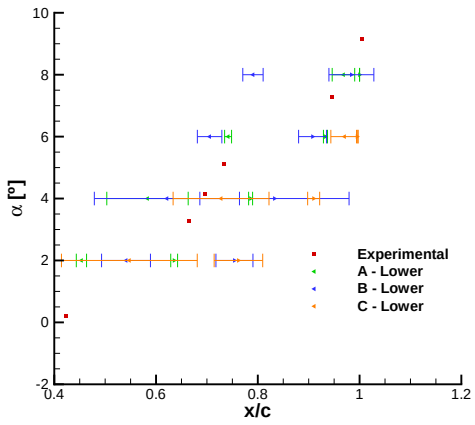

Figure 5: Transition location for the NACA 0012 airfoil, lower surface.

No case exhibits reasonable accuracy for both surfaces. It would appear that the effect of the x_{inlet} is of higher importance than the inlet eddy viscosity, since transition occurs later for conditions C. However, for the remaining angles, conditions B exhibit transition in the lower surface earlier than case C, while the order remains the same as before for the upper surface, indicating influence from the pressure gradient.

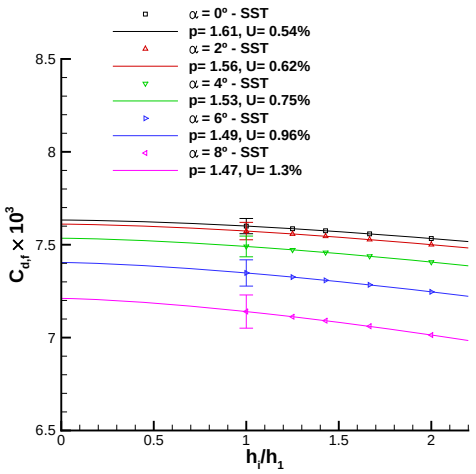

Figure 6: Friction drag uncertainty estimate for the NACA 0012 airfoil, SST model.

The uncertainty estimation for the friction drag is presented in figures 6 and 7. All of the LCTM calculations predict lower values for the friction drag than those of the SST model, which is to be expected since a considerable part of the flow is laminar. The change of the friction drag with the angle of attack is not simple since there are two opposing effects: the contribution from the upper surface tends to increase since transition moves upstream, while the reverse occurs in the lower surface. Overall, the numerical uncertainties are low, although the LCTM calculations present slightly higher values.

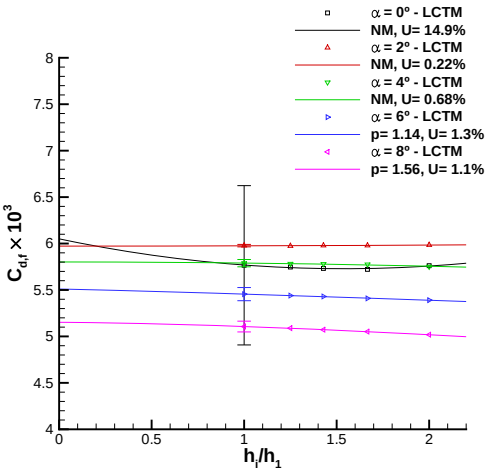

Figure 7: Friction drag uncertainty estimate for the NACA 0012 airfoil, LCTM

The SST calculations exhibit slightly higher values for the lift coefficient than those obtained with the transition model, as evidenced by figure 8.

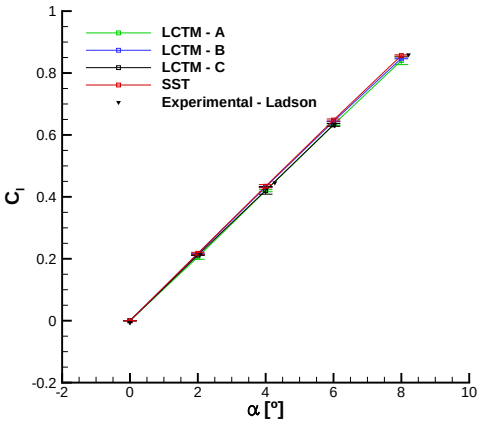

Figure 8: Lift force for the NACA 0012 airfoil.

The drag polar is shown in figure 9, with the estimated numerical uncertainty. The SST model presents the highest value, followed by conditions A of the LCTM calculations. It is important to remember that the accuracy shown by case A is not fortuitous, since the turbulent conditions were chosen in order to match the drag for $\alpha = 0°$. As expected, cases B and C exhibit lower values, since transition is delayed, and the difference to case A is quite significant. All cases present high numerical uncertainties.

4.2. NACA 66-018

Figure 10 shows the pressure coefficient distribution for $\alpha = 0°$. Overall, the results obtained are slightly below the available experimental data, but exhibit the same trend. Including the transition model seems to affect very little

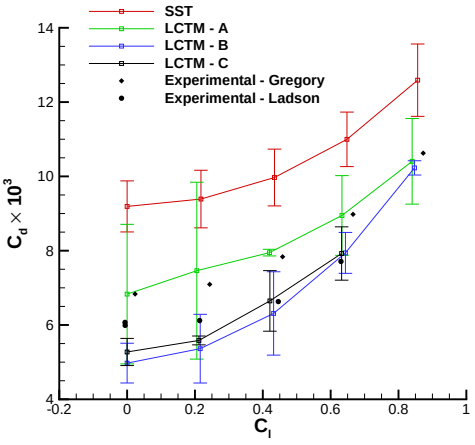

Figure 9: Drag force for the NACA 0012 airfoil.

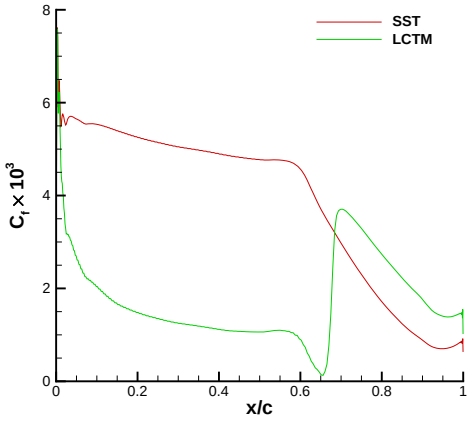

Figure 11: Skin friction for the NACA 66-018 airfoil, $\alpha = 0°$.

the pressure coefficient.

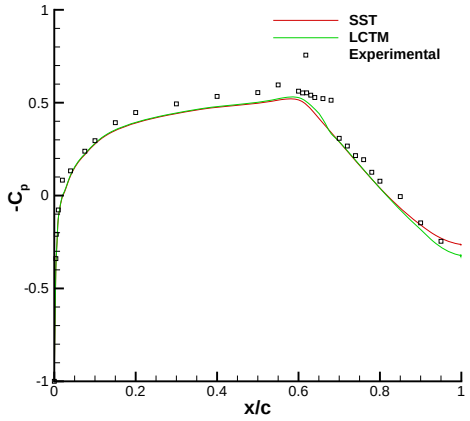

Figure 10: Pressure coefficient for the NACA 66-018 airfoil, $\alpha = 0°$.

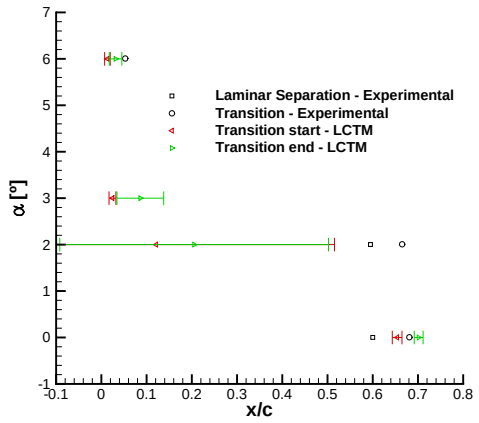

Figure 12: Transition location for the NACA 66-018 airfoil.

The skin friction distribution is shown in Figure 11. Here, the differences between the SST and LCTM calculations are significant: fully turbulent flow occurs in both the upper and lower surface of the airfoil when using the SST model, as is to be expected. When the transition model is used, a significant portion of the airfoil is in the laminar regime.

The available experimental data for transition are not in accordance with the obtained results - Figure 12.

Figure 13 shows the uncertainty estimation for the friction components of the drag force. The SST calculations provide a higher value for the friction drag, consequence of the fully turbulent flow condition which decreases slightly with the increase of the angle of attack, with low uncertainties. Using the transition model results in lower friction drag, increasing along with the angle of attack due to the upstream movement of transition on the upper surface, and significantly higher numerical uncertainty.

As should be expected, the drag coefficient obtained with the transition model is significantly lower than that of the SST model. However, the model failed to capture the experimental trend for the drag coefficient.

4.3. Eppler 387

4.3.1 $\mathbf{Re} = 3 \times 10^5$

Figures 15 and 16 show the pressure coefficient and skin friction distribution for the lowest angle of attack. The LCTM calculations exhibit a laminar separation bubble on each side of the airfoil, which is responsible for triggering transition, unlike when using the SST model in which natural transition always takes place. Differences in the pressure distribution are only found near the beginning of the adverse pressure gradient and in the separated flow zones. Regarding the lower surface, although the LCTM calculations also suggest separation-induced transition, such is

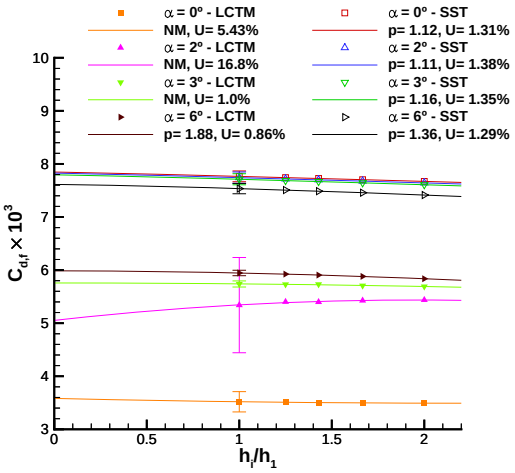

Figure 13: Uncertainty estimate for friction drag for the NACA 66-018 airfoil.

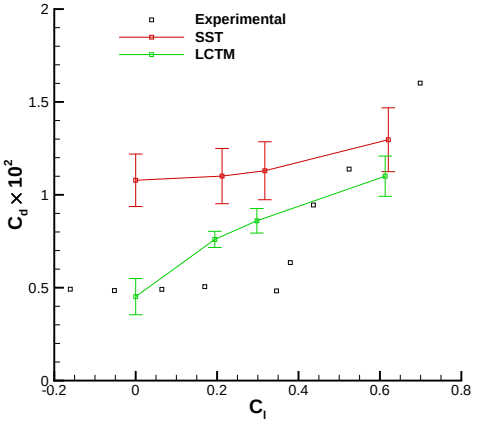

Figure 14: Drag for the NACA 66-018 airfoil.

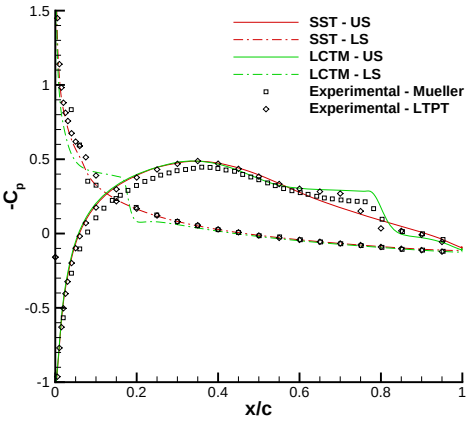

Figure 15: Pressure coefficient for $\alpha = -2°$ for the Eppler 387 airfoil at $Re = 3 \times 10^5$.

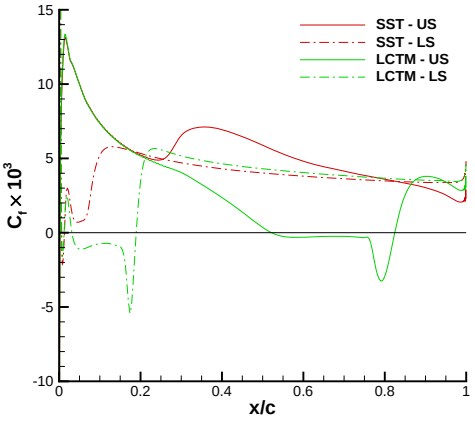

Figure 16: Skin friction for $\alpha = -2°$ for the Eppler 387 airfoil at $Re = 3 \times 10^5$.

not in accordance with the experimental data.

In all cases there seems to be good agreement between the numerical and experimental pressure coefficient distribution, although one set of experimental data [27] consistently presents slightly higher pressure in the lower surface. This may be due to blockage effects, since the other set of points do not exhibit the same behaviour.

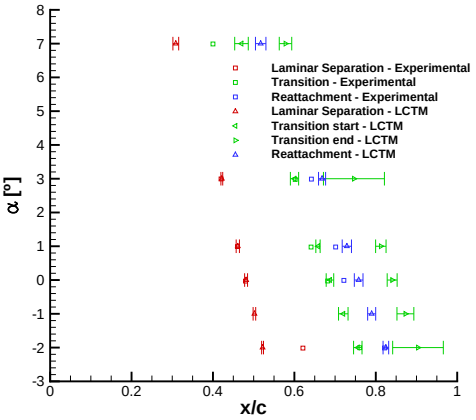

Figure 17: Transition chordwise location for the Eppler 387 airfoil at $Re = 3 \times 10^5$.

Figure 17 shows the experimental and numerical location of the points of interest concerning transition and the separated flow region, with the respective numerical uncertainty. A larger bubble is always obtained for the numerical solution. The location of laminar separation exhibits the smallest numerical uncertainty when compared to the other relevant points. The onset of transition as well as turbulent reattachment also exhibit a small uncertainty, while the end of transition presents the largest, a consequence of non-monotonic behaviour caused by the coarsest grids.

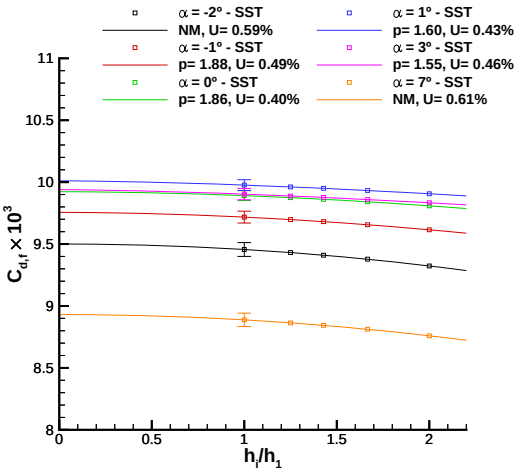

Figure 18: Friction drag uncertainty estimate for the Eppler 387 airfoil at $Re = 3 \times 10^5$, SST model.

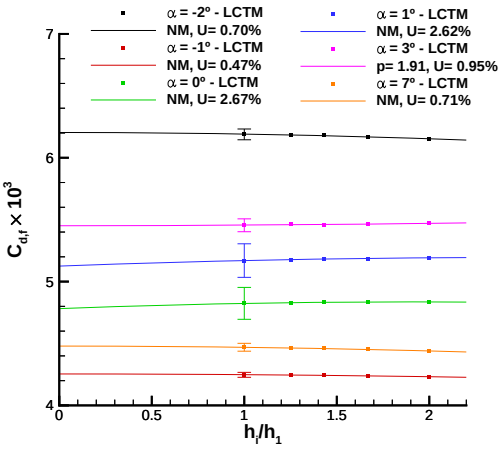

Figure 19: Friction drag uncertainty estimate for the Eppler 387 airfoil at $Re = 3 \times 10^5$, LCTM.

The friction component of drag is presented in Figures 18 and 19. The predictions obtained when using the transition model are always lower than when using the SST model, due to delayed transition and the appearance of the laminar separation bubbles. The numerical uncertainties are very low for both models, generally lower than 1%.

The SST solutions constantly predict higher drag than the experimental data, a consequence of failing to capture the laminar separation bubble - Figure 20. The values estimated by the transition model are much closer to the experimental data. In general, the transition model presents higher uncertainties than calculations performed with the SST model, for both the lift and drag, namely the two highest angles of attack exhibit values higher than 10%.

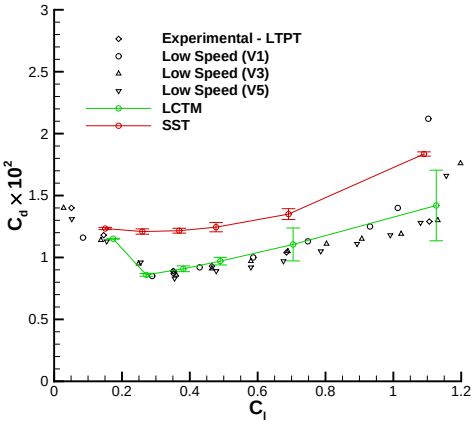

Figure 20: Drag force for the Eppler 387 airfoil at $Re = 3 \times 10^5$.

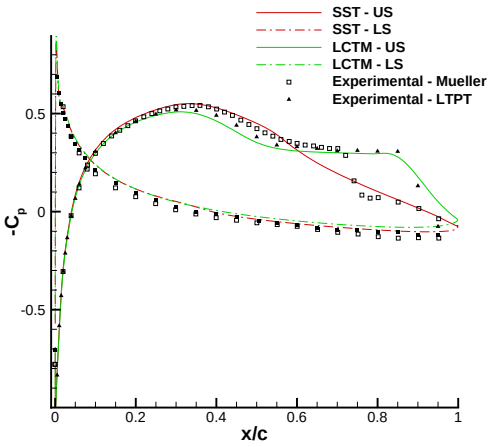

Figure 21: Pressure coefficient for $\alpha = -1°$ for the Eppler 387 airfoil at $Re = 1 \times 10^5$.

4.3.2 Re $= 1 \times 10^5$

Figures 21 and 22 present the skin friction and pressure distribution for the Eppler 387 airfoil at a Reynolds number of 1×10^5. The pressure coefficient differs slightly in the upper surface between the two models, both in the region where a laminar separation bubble is located, as well as in the region before it. For the lower surface, the two pressure distributions are almost overlapping. Similarly to the previous section, the experimental pressure data show some differences particularly in the lower surface and again the numerical solution is more in accordance with the LTPT data [28].

Unlike the other tested Reynolds number, the agreement between the experimental and numerical position of laminar separation is not as good - figure 23. The numerical prediction for turbulent reattachment is also worse for this Reynolds number. One striking consequence from the combined behaviour of the separation and reattach-

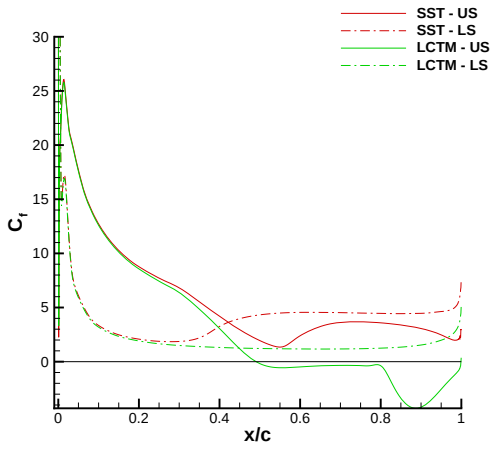

Figure 22: Skin friction for $\alpha = -1°$ for the Eppler 387 airfoil at $Re = 1 \times 10^5$.

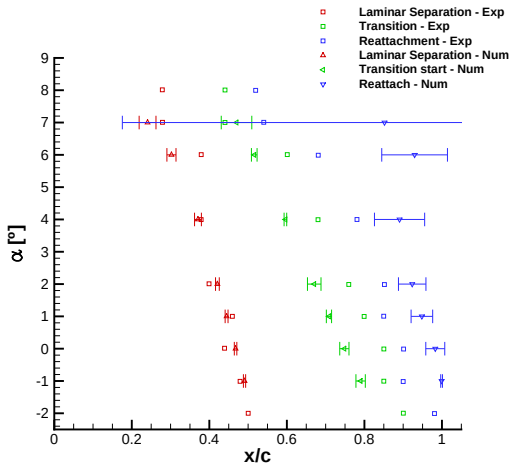

Figure 23: Transition chordwise location for the Eppler 387 airfoil at $Re = 1 \times 10^5$.

ment locations is in the size of the bubble: the numerical solution always exhibits a larger separated region than the wind-tunnel data, particularly for the higher angles.

The total drag obtained from the SST model is much lower than both experimental data and transition model calculations - Figure 24. The latter matches well with the former for the lower angles, but clearly overpredicts the drag for the higher angles when the effect of the bubble should be decreasing. Much like before, the numerical uncertainty is higher for the LCTM case and a clear growth is seen when increasing the angle of attack. This suggests the grids are not fine enough for these angles, as monotonic convergence was obtained for these cases.

5. Conclusions

In this thesis the effect of transition modelling on the flow for three different airfoils was analyzed. The $\gamma - Re_\theta$ transition model of Langtry and Menter was used and the results were compared with baseline calculations using only

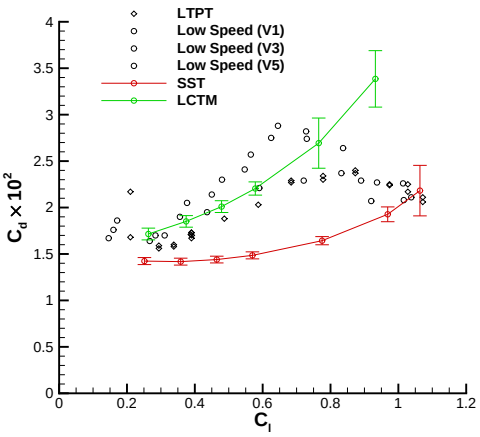

(b) Drag Polar

Figure 24: Drag force for the Eppler 387 airfoil at $Re = 1 \times 10^5$.

the SST $k - \omega$ turbulence model and available experimental data. The three airfoils tested were the NACA 0012, NACA 66-018 and the Eppler 387 airfoil.

The work performed provided the following conclusions:

- The main work showed that the transition model is not as numerically robust as the SST turbulence model: iterative convergence becomes much more difficult.

- The transition model is much more sensitive to the inlet turbulence settings, namely the eddy viscosity, unlike the SST model. This higher sensitivity is aggravated by the turbulent decay that is greatly overestimated by common turbulence models, meaning that information regarding turbulence should also be provided in experimental testing, in order to extract proper conclusions regarding model validation.

- The uncertainty estimation for the pressure and friction components of drag and lift showed that higher discretization errors are obtained when the $\gamma - Re_\theta$ model is used and can reach extremely high values in some cases. Transition can occur at regions where the grid is not sufficiently refined in the streamwise direction, causing non-monotonic behaviour.

- The calculations on the Eppler 387 airfoil showed that the transition model correctly predicted laminar separation but causes reattachment to occur too late. Separation induced transition is the case that shows the best iterative convergence properties.

- On the contrary, cases where natural transition is expected, such as in the NACA 0012 airfoil, are highly dependent on the combination of turbulence boundary conditions and turbulence decay.

- Overall, the calculations with the transition model showed an improvement in accuracy when compared to the SST solutions. The skin friction curves showed clear differences, but a clear comparison is not evident since no experimental data was available. The lift coefficient suffered little change, while the drag showed a clear improvement for most cases.

Future work on this topic should include a more detailed study on the effect of the inlet turbulent variables, as their specification seems to have a major impact on the solution. This is valid not only for cases where natural transition takes place, but also for geometries were laminar separation bubbles are formed. It would be interesting to compare the $\gamma - Re_\theta$ model with other available alternatives for transition modelling, or even implementations with other turbulence models. Finally, the behaviour of the model in three-dimensional problems is also worthy of some attention, given the higher complexity of the boundary layer in these situations.

References

[1] J. H. Ferziger and M. Peric. *Computational methods for fluid dynamics*. 3rd Ed., Springer, 2012.

[2] T. J. Mueller and J. D. DeLaurier. Aerodynamics of small vehicles. *Annual Review of Fluid Mechanics*, 35(1):89–111, 2003.

[3] T. J. Mueller. Low Reynolds number vehicles. Technical report, DTIC Document, 1985.

[4] W. Shyy, Y. Lian, J. Tang, D. Viieru, and H. Liu. *Aerodynamics of low Reynolds number flyers*, volume 22. Cambridge University Press, 2007.

[5] A. M. O. Smith and N. Gamberoni. *Transition, pressure gradient and stability theory*. Douglas Aircraft Company, El Segundo Division, 1956.

[6] J. L. Van Ingen. A suggested semi-empirical method for the calculation of the boundary layer transition region. Technical report, Delft University of Technology, 1956.

[7] M. Drela and M. B. Giles. Viscous-inviscid analysis of transonic and low Reynolds number airfoils. *AIAA journal*, 25(10):1347–1355, 1987.

[8] F. R. Menter, R. B. Langtry, S. R. Likki, Y. B. Suzen, P. G. Huang, and S. Völker. A correlation-based transition model using local variablespart i: model formulation. *Journal of turbomachinery*, 128(3):413–422, 2006.

[9] ReFRESCO, 2015. URL `http://www.refresco.org`.

[10] H. Schlichting and K. Gersten. *Boundary-layer theory*. Springer, 2000.

[11] M. V. Morkovin. On the many faces of transition. In *Viscous drag reduction*, pages 1–31. Springer, 1969.

[12] R. E. Mayle. The role of laminar-turbulent transition in gas turbine engines. *Journal of Turbomachinery*, 113(4):509–536, 1991.

[13] D. D. Pasquale, A. Rona, and S. J. Garrett. A selective review of CFD transition models. 39th AIAA Fluid Dynamics Conference, 2009, San Antonio, Texas, American Institute of Aeronautics and Astronautics, June 2009.

[14] R. G. Jacobs and P. A. Durbin. Simulations of bypass transition. *Journal of Fluid Mechanics*, 428:185–212, 2001.

[15] D. C. Wilcox. *Turbulence Modeling for CFD*. 2nd Edition, DCW Industries, Inc., 2004.

[16] A. M. Savill. Some recent progress in the turbulence modelling of bypass transition. *Near-wall turbulent flows*, pages 829–848, 1993.

[17] J. Steelant and E. Dick. Modelling of bypass transition with conditioned Navier-Stokes equations coupled to an intermittency transport equation. *International journal for numerical methods in fluids*, 23(3):193–220, 1996.

[18] R. B. Langtry and F. R. Menter. Correlation-based transition modeling for unstructured parallelized computational fluid dynamics codes. *AIAA journal*, 47(12):2894–2906, 2009.

[19] C. Seyfert and A. Krumbein. Evaluation of a correlation-based transition model and comparison with the en method. *Journal of Aircraft*, 49(6):1765–1773, 2012.

[20] L. Eça. Grid generation tools for structured grids. Technical Report Report D72-18, Instituto Superior Técnico, 2003.

[21] R. B. Langtry. *A correlation-based transition model using local variables for unstructured parallelized CFD codes*. PhD thesis, Universität Stuttgart, 2006.

[22] L. Eça and M. Hoekstra. A procedure for the estimation of the numerical uncertainty of CFD calculations based on grid refinement studies. *Journal of Computational Physics*, 262: 104–130, 2014.

[23] P. R. Spalart and C. L. Rumsey. Effective inflow conditions for turbulence models in aerodynamic calculations. *AIAA journal*, 45(10):2544–2553, 2007.

[24] N. Gregory and C. L. OReilly. Low-speed aerodynamic characteristics of NACA 0012 aerofoil section, including the effects of upper-surface roughness simulating hoar frost. Technical report, 1970.

[25] C. Ladson. Effects of independent variation of Mach and Reynolds numbers on the low-speed aerodynamic characteristics of the NACA 0012 airfoil section. Technical report, 1988.

[26] D. E. Gault. *An experimental investigation of regions of separated laminar flow*. Number 3505. National Advisory Committee for Aeronautics, 1955.

[27] G. M. Cole and T. J. Mueller. Experimental measurements of the laminar separation bubble on an Eppler 387 airfoil at low Reynolds numbers. *NASA STI/Recon Technical Report N*, 90: 15380, 1990.

[28] R. J. Mcghee, B. S. Walker, and B. F. Millard. Experimental results for the Eppler 387 airfoil at low Reynolds numbers in the Langley low-turbulence pressure tunnel. 1988.

[29] M. S. Selig, J. J. Guglielmo, A. P. Broeren, and Gigure P. *Summary of low speed airfoil data*, volume 1. SoarTech, 1995.

[30] M. S. Selig, C. A. Lyon, A. P. Broeren, Gigure P., and Gopalarathnam A. *Summary of low speed airfoil data*, volume 3. SoarTech, 1997.

[31] G. A. Williamson, B. D. McGranahan, B. A. Broughton, R. W. Deters, J. B. Brandt, and M. S. Selig. *Summary of low speed airfoil data*, volume 5. SoarTech, 2012.

[32] R. M. A. Lopes. Calculation of the flow around hydrofoils at moderate Reynolds numbers. Master's thesis, Instituto Superior Técnico, 2015.